sustainability

MDPI

Article

Preparation and Performance Study of Waste Straw-Based Composites for High-Value Resource Cycling

Shasha Jin [1], Yafei Fan [2,3,4] and Yi Liu [2,3,4,*]

[1] School of Jewellery, Birmingham City University, Birmingham B1 3PA, UK
[2] College of Materials Science and Technology, Beijing Forestry University, Beijing 100083, China
[3] Key Laboratory of Wood Material Science and Application, Ministry of Education, Beijing Forestry University, Beijing 100083, China
[4] Beijing Key Laboratory of Wood Science and Engineering, Beijing Forestry University, Beijing 100083, China
* Correspondence: jruihe7@163.com

Abstract

To address the low utilization rate of straw and environmental pollution caused by traditional processing methods, this study developed a novel composite material based on straw for manufacturing outdoor furniture. Designed to achieve high-value recycling of agricultural waste and enhance the durability and sustainability of outdoor materials, the straw is treated with alkali and processed using an MDI curing system, with the addition of ZnO to enhance functional properties. Characterization of material properties was performed using contact angle measurements, UV-visible spectroscopy, and mechanical testing. The results indicate that a water contact angle of 93.51° was achieved for the composite material at a ZnO content of 6 wt.%, demonstrating excellent hydrophobicity. The introduction of ZnO reduced light absorption, indicating that the material exhibits superior stability in interior and exterior environments. The synergistic interaction between ZnO and straw fibers, along with the resulting active free radicals (·OH), endows this material with hydrophobic and UV-resistant properties. This composite material combines excellent mechanical strength with environmental friendliness, offering broad prospects in the field of sustainable outdoor furniture manufacturing.

Keywords: straw; material modification; mechanical properties; UV resistance

1. Introduction

The global construction boom has led to a sharp increase in timber demand, driving persistent deforestation and resulting in severe biodiversity loss and ecological degradation [1,2]. Developing sustainable alternatives to timber is essential for ensuring resource security and mitigating climate change. Wood-based composites, which combine desirable material properties with efficient resource utilization, represent a promising solution. Current research increasingly focuses on renewable and low-cost biomass feedstocks to partially replace wood and reduce reliance on forest resources. Among these, agricultural residues such as corn stalks are abundant, cellulose-rich, and highly suitable as alternative raw materials [3–6]. However, most maize straw is currently either buried or burned, causing significant environmental pollution. The accumulation of unused straw in fields not only occupies land as solid waste but also represents a loss of valuable biomass resources. Therefore, converting straw into value-added materials is crucial for advancing sustainable agriculture and environmental protection.

Check for updates

Academic Editor: Antonio Caggiano

Received: 20 February 2026
Revised: 22 March 2026
Accepted: 23 March 2026
Published: 1 April 2026

Copyright: © 2026 by the authors. Licensee MDPI, Basel, Switzerland. This article is an open access article distributed under the terms and conditions of the Creative Commons Attribution (CC BY) license.

Corn stalks are characterized by high yield, low cost, and broad application potential in the construction and composite materials industries. Their chemical composition—rich in cellulose, hemicellulose, and lignin—is similar to that of wood and typical of lignocellulosic materials. Consequently, corn stalks have strong potential to replace traditional wood in engineered panel manufacturing [7–9]. Nevertheless, straw presents several limitations in such applications. The presence of a surface wax layer and hydrophobic components significantly hinders adhesive wetting and chemical bonding, leading to weak interfacial adhesion and inferior mechanical performance [10–13]. In addition, the polysaccharides and cellulose in straw are susceptible to biodegradation and aging under high-temperature and high-humidity conditions, which compromises the water resistance, durability, and long-term safety of the resulting panels [14–16]. Enhancing the durability and oxidation resistance of straw-based composites thus remains a key research priority for their application in engineered wood products. To address these challenges, extensive studies have been conducted, including chemical modification, doping, and particle size reduction through ball milling. For instance, Anam et al. [17] developed a lightweight thermal insulation material using corn straw and demonstrated that straw incorporation reduces thermal conductivity while improving flexural and tensile moduli. Bheel et al. [18] showed that straw ash rich in amorphous SiO_2, obtained through thermochemical or physical modification, can serve as an effective reinforcing phase or functional filler, significantly enhancing the mechanical strength and durability of composites. Furthermore, agricultural straw can be converted into mesoporous silica for improving the thermal and acoustic performance of epoxy nanocomposites or used directly as a pozzolanic substitute in cement, highlighting its dual potential in sustainable material development [19,20]. In addition to structural reinforcement, improving the photo-oxidation resistance of straw-based materials is equally critical. However, most existing treatments are insufficient to effectively suppress photodegradation induced by ultraviolet (UV) and visible light, leading to oxidation and reduced service life of engineered panels. Although inorganic nanoparticles such as TiO_2 can provide UV shielding, their photocatalytic activity may accelerate the photo-oxidative degradation of polymer matrices [21,22]. Glazar et al. [23] demonstrated that TiO_2 in $Ag/TiO_2/CN$ nanocomposites generates reactive oxygen species (e.g., O_2^-) under illumination, which effectively degrade Rhodamine B dye. This finding suggests that incorporating TiO_2 directly into polymer systems such as PLA may induce undesired degradation of polymer chains. Organic UV absorbers and hindered amine light stabilizers (HALS) are commonly used to enhance photostability; However, issues such as photodegradation of the stabilizers themselves and their migration within the matrix remain unresolved [24,25]. Emerging nanomaterials, including carbon quantum dots, offer new possibilities for transparent coatings due to their excellent full-spectrum UV absorption and high photostability. Nevertheless, their long-term protective mechanisms and scalability in straw-based composite systems require further investigation [26,27]. Electrogalvanized sludge, an underutilized solid waste, provides a novel approach for modifying straw-based composites and enhancing their antioxidant properties. Its primary components, $Zn(OH)_2$ and ZnO, are of particular interest [28]. ZnO is not only a widely used antioxidant but also a wide-bandgap semiconductor capable of effectively absorbing and scattering UV radiation (especially in the UVA and UVB regions). In addition, it exhibits antibacterial and antifungal properties through the generation of reactive oxygen species. Owing to its structural stability and resistance to degradation, ZnO can improve both the mechanical performance and oxidative stability of straw-based materials [29–34].

Based on the above considerations, this study employs alkali treatment to pretreat straw powder surfaces, thereby improving their compatibility with synthetic resins. Subsequently, ZnO is incorporated to impart enhanced antioxidant properties, enabling the

fabrication of high-performance composites. A combination of characterization techniques, including scanning electron microscopy (SEM), X-ray diffraction (XRD), and UV–Vis spectroscopy, was used to investigate the composites. These analyses elucidate the dual mechanisms of interfacial modification and performance enhancement from both microstructural and chemical bonding perspectives. This work not only provides critical data and novel insights for promoting the large-scale utilization of agricultural waste fibers but also establishes a solid foundation for the high-value application of straw resources.

2. Experiment

2.1. Material

The materials and chemicals used are listed below: Straw powder (purchased from Shandong Province, China), Isocyanate (MDI, Sinopharm Reagent, Beijing, China), Paraffin emulsion (Aladdin, Shanghai, China), Sodium hydroxide (Aladdin, Shanghai, China), Electroplating sludge, Ethanol (Aladdin, Shanghai, China).

2.2. Fabrication of Straw-Based Composite Materials

2.2.1. Preparation of WPC Samples

Pretreatment of straw: To improve the interfacial compatibility between straw and the matrix and enhance the performance of engineered wood-based panels, straw pretreatment was conducted. First, the straw was rinsed with distilled water to remove soil and other impurities. It was then soaked in a 15 wt.% sodium hydroxide solution for 2 h to remove surface wax, silica, and partial hemicellulose. This treatment exposes more hydroxyl groups of cellulose, thereby improving surface wettability and reactivity. Subsequently, the treated straw was dried in an oven at 80 °C until its moisture content was below 1%. Finally, the dried straw was ground into powder using a crusher and sieved with a vibrating screen to obtain the target particle size of 200 mesh.

Electroplating sludge: 20 g of electroplating sludge, mainly composed of $Zn(OH)_2$, $Fe(OH)_3$, CaO, and Al_2O_3, was weighed and added to 0.1 mol/L sulfuric acid. Acid leaching was conducted at 75 °C under continuous stirring to extract Zn, Fe, Al, Ca and other heavy metal ions into the aqueous solution. Glucose was introduced as a reducing agent into the acid leachate, followed by hydrothermal treatment at 160 °C for 2 h. This procedure promoted the formation of a mixed precipitate rich in Fe_2O_3 and Al_2O_3, while most Zn species remained in the solution. Meanwhile, Ca^{2+} reacted with sulfate ions to form sparingly soluble calcium sulfate (gypsum) precipitate. Subsequently, 0.15 mol/L NaOH solution was added to the purified zinc-rich solution to adjust the pH to 8, leading to the precipitation of $Zn(OH)_2$. The resulting zinc hydroxide precipitate was washed, dried, and calcined at 300 °C to obtain high-purity zinc oxide. Characterization and analysis verified that the total content of the major impurities (Fe, Al, and Ca) was below 0.1%.

2.2.2. Preparation of Straw Powder-ZnO Composite

Pretreated straw powder (20 g) was mixed with 8 wt.% MDI adhesive (1.6 g) and 4 wt.% paraffin emulsion (0.5 g) until a uniform coating was achieved. Pre-prepared ZnO (2 wt.%, 0.4 g) was introduced during mixing. The mixture was uniformly deposited into a release-agent-treated mold and cold-prepressed to form a manageable mat. Hot pressing was conducted at 165 °C for 10 min. After natural cooling to room temperature, the panels were cured for at least 24 h to eliminate internal stresses. Figure 1 shows the experimental process. Three additional sets of specimens were prepared under identical conditions with ZnO contents of 0 wt.%, 4 wt.%, and 6 wt.% for comparison, shown in Table 1.

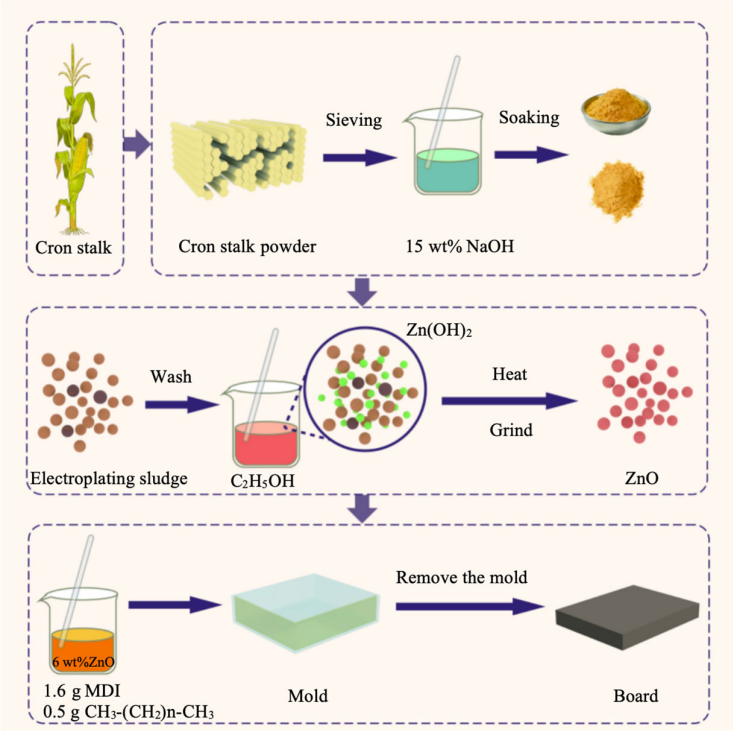


Figure 1. Experimental flowchart of straw powder—ZnO composite.

Table 1. Summary table of the formulations.

Materials	Straw Powder	ZnO
0 wt.%	20 g	0 g
2 wt.%	20 g	0.4 g
4 wt.%	20 g	0.8 g
6 wt.%	20 g	1.2 g

2.3. Materials Characterization

The microstructure of the straw powder-ZnO composite was characterized using a scanning electron microscope (SEM, Hitachi S4800, Tokyo, Japan). Phase composition was determined via X-ray diffraction (XRD, X'Pert PRO MPD, Almelo, The Netherlands). The chemical bonding states of the composites were analyzed using X-ray photoelectron spectroscopy (XPS, Thermo K-Alpha, Loughborough, UK). Thermal stability was evaluated by means of thermogravimetric analysis (TGA/DSC, Rigaku, Tokyo, Japan). Compressive properties were measured using an electronic universal testing machine (UTM, CMT6103, Sansi Yongheng Technology (Zhejiang) Co., Ltd., Ningbo City, China). UV resistance was assessed using a UV–visible spectrophotometer over the wavelength range of 200–800 nm. Surface hydrophobicity was evaluated through water contact angle measurements. The lattice structure of the composites was examined by means of transmission electron microscopy (TEM, FEI Tecnai F20, FEI Company, Hillsboro, OR, USA). The presence of active free radicals was analyzed using an electron paramagnetic resonance (EPR) spectrometer (Bruker EMX Plus, Rheinstetten, Germany).

3. Results and Discussion

3.1. Structural Analysis of Straw-Based Composite Materials

Figure 2 presents the XRD patterns of straw-derived composites incorporated with different loadings of ZnO. The pristine straw powder shows two characteristic broad and weak diffraction peaks at 2θ = 19.7° and 43.6°, corresponding to its typical amorphous

cellulose structure. These two broad peaks are typical of biomass materials, reflecting the amorphous and semi-crystalline structure dominated by cellulose, hemicellulose, and lignin. With increasing ZnO doping concentration, a series of sharp and intense diffraction peaks gradually emerge and become significantly stronger at 2θ = 31.8°, 34.4°, 36.3°, 47.5°, 56.6°, 62.9°, and 66.4°, which can be well indexed to the (100), (002), (101), (102), (110), (103), and (200) crystal planes of hexagonal wurtzite-structured ZnO (PDF#36-1451). The peak intensity of ZnO characteristic diffraction signals increases monotonically with the increase of ZnO loading, indicating that the crystallinity of ZnO in the composites is gradually enhanced. The incorporation of ZnO not only dilutes the relative mass fraction of cellulose but also generates strong interfacial interactions between ZnO and straw fibers, which may disrupt the ordered arrangement of cellulose chains, reduce the crystallite size or overall crystallinity of cellulose, and further lead to the attenuation of its diffraction peak intensity. No impurity peaks are detected in all composite samples, confirming the high phase purity and good crystallization of the loaded ZnO. The above XRD results clearly verify that ZnO has been successfully immobilized onto the straw matrix, and the crystalline phase of ZnO is uniformly compounded with the cellulose-based structure of straw.

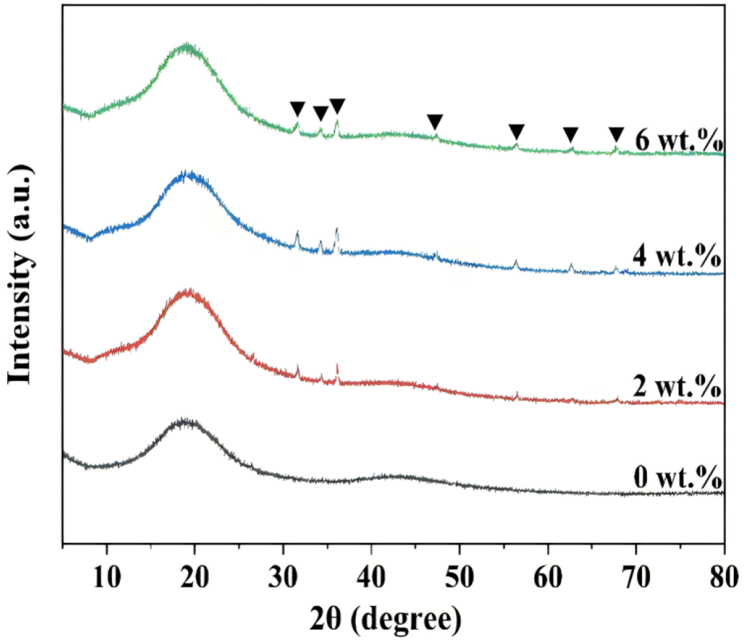


Figure 2. XRD Patterns of Straw-Based Composites at Different ZnO Content Levels.

To further clarify the influence of ZnO addition on the interfacial modification of straw-based composites and the corresponding changes in internal microstructure, the specimens were observed using scanning electron microscopy (SEM). Figure 3 shows the SEM transverse cross-sectional morphologies of straw-based composites at different ZnO loading levels (0, 2, 4, and 6 wt.%), systematically revealing the modifying role of ZnO on the interface and microstructure of the composites. In the absence of ZnO (Figure 3a,b), the cross-section exhibits a rough surface and is riddled with numerous pores, indicating weak interfacial bonding within the rice straw fibers and the presence of substantial defects. After adding 2 wt.% ZnO (Figure 3c,d), the quantity of pores is reduced. As revealed by microstructural analysis, ZnO particles were anchored on the fiber surface and interfacial domains, acting as physical fillers and providing effective interfacial bridging between the fiber and matrix. This effect contributed to the improved interfacial compatibility of the composites. At a ZnO content of 4 wt.% (Figure 3e,f), the fracture surface exhibited a wrinkled layered morphology with increased roughness and refined

pore structures. This is attributed to interfacial enrichment of ZnO, which strengthened interphase mechanical interlocking and promoted a more tortuous crack propagation path. When the ZnO loading reached 6 wt.% (Figure 3g,h), the cross-section became dominated by compact, flat, and dense regions, with macroscopic pores nearly eliminated. ZnO particles were uniformly dispersed without obvious agglomeration. The enhanced interfacial interaction between ZnO and straw components promoted plastic deformation and interfacial fusion, forming a thin coating layer that smoothed wrinkles and pores and yielded a more uniform morphology. Meanwhile, increased ZnO content facilitated better dispersion under high-speed stirring, allowing ZnO to effectively fill internal defects and greatly improve interfacial adhesion and structural compactness. Overall, increasing ZnO content drove the transformation of the composite from a porous and loose structure to a dense and homogeneous one. Through interfacial modification and defect filling, ZnO optimized interfacial bonding between straw and the matrix, establishing a favorable microstructural basis for performance enhancement.

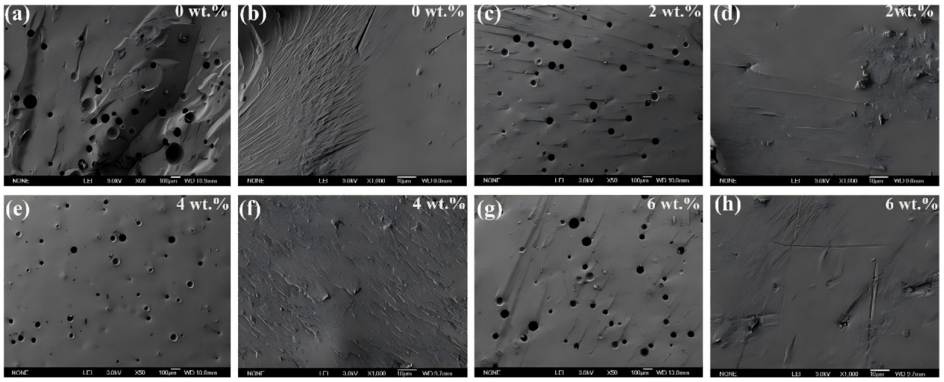


Figure 3. SEM Images of Straw-Based Composites with Different ZnO Additions, (**a**,**b**) 0 wt.%; (**c**,**d**) 2 wt.%; (**e**,**f**) 4 wt.%; (**g**,**h**) 6 wt.%.

3.2. Performance Analysis of Straw-Based Composite Materials

Figure 4a displays the UV-vis absorption spectra of straw-based composites with varying ZnO doping levels (0–6 wt.%) across the 200–800 nm wavelength range. In the UV region (200–400 nm), all samples exhibited marked absorption, and the absorption intensity systematically increased with rising ZnO content. Such behavior is attributed to the bandgap of ZnO, facilitating the transition between the valence band and the conduction band. A broad absorption band is observed in the 365–405 nm wavelength range, which corresponds to the edge absorption feature of ZnO. It aligns with the characteristic absorption edge of hexagonal zinc blende ZnO and the potential exciton absorption behavior, confirming that ZnO is uniformly dispersed in the composite and maintains its crystal structure [35]. These results further confirm the successful loading and effective incorporation of ZnO. In the visible light region (400–800 nm), the absorption intensity of the composite generally exhibits a decrease with rising ZnO content. In particular, samples with higher doping concentrations (6 wt.%) exhibited a significantly reduced absorption background in the visible light region. This reduction appears to stem from the scattering of visible light by ZnO particles and improved optical matching at the interface with the substrate. These two factors reduce the light trapping effect and absorption losses within the composite material. Addition of ZnO contributes to reducing the absorption of the composite panel in the visible light region, which may mitigate light-induced thermal effects and improve the thermal stability of the material in outdoor applications.

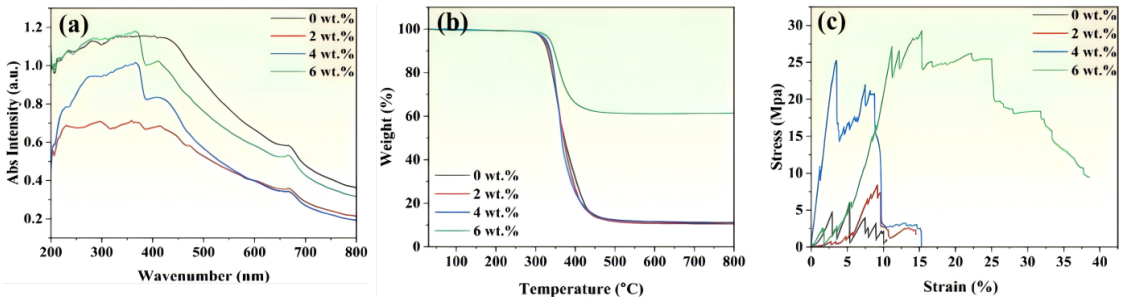


Figure 4. (**a**) UV-Vis Absorption Spectra, (**b**) Thermal Analysis, and (**c**) Compressive Stress–Strain Curves of Straw-Based Composites with Different ZnO Additions.

Figure 4b shows the thermogravimetric (TG) curves of straw-based composites with different ZnO contents (0, 2, 4, and 6 wt.%) in a N_2 atmosphere. It systematically analyzes the influence of ZnO on the thermal degradation behavior and stability of the composites. All samples exhibited a similar three-stage thermal decomposition process. This consistency indicates that the thermal degradation mechanisms are fundamentally similar across all samples. Nevertheless, ZnO content significantly affects the weight loss behavior at each degradation stage and the final char residue. In the first stage (30–300 °C), a weight loss of approximately 2% was observed, mainly arising from the desorption of adsorbed water, small-molecule volatiles, and residual solvents. During this stage, weight loss behavior is consistent for samples with various ZnO loadings, indicating negligible effects of ZnO on corresponding thermal processes. The second stage (300–500 °C) represents the primary thermal decomposition region. Within this temperature interval, thermal cleavage occurs for ester and ether moieties in the epoxy resin matrix, and intensive degradation takes place for cellulose and hemicellulose components in straw fibers. All samples underwent pronounced weight loss during this stage. Increasing ZnO loading correlates with a moderately suppressed weight-loss rate and a slight elevation in the thermal decomposition end-temperature. This observation confirms that ZnO hinders the thermal cleavage of polymer chains to a certain degree via physical barrier effects and interfacial interactions within the composite. ZnO particles impede the diffusion of thermally decomposed products and reinforce the thermal stability of the composite matrix. In the third decomposition stage (>500 °C), associated with the carbonization/stabilization regime, the residual carbon content of the samples containing 0–4 wt.% ZnO remained essentially constant at ~15%, suggesting that ZnO incorporation within this loading window has little impact on the final char yield. Strikingly, increasing the ZnO loading to 6 wt.% led to a dramatic rise in the residual carbon content to 63.78%. This behavior cannot be accounted for solely by the inherent thermal robustness of ZnO and its contribution to the condensed-phase residue. Instead, the result points to a threshold-like effect at higher ZnO loadings, where the formation of a more continuous inorganic protective network more effectively impedes thermal transport and volatile diffusion, thereby substantially enhancing char preservation. The reinforced barrier network effectively inhibits the release of volatile pyrolysis products while concurrently promoting the formation and stabilization of the carbon layer. These synergistic effects markedly enhance the material's thermal stability and carbonization efficiency at elevated temperatures. In particular, ZnO incorporation at high loadings (6 wt.%) substantially retards thermal decomposition by serving as a robust physical barrier and facilitating the development of a continuous carbonaceous layer, thereby significantly improving both the composite's thermal resilience and char yield.

Subsequently, the compressive stress–strain analyses were conducted on straw-based composites with varying ZnO contents (0–6 wt.%), systematically revealing the mechanism by which ZnO influences the mechanical behavior of the materials. As shown in Figure 4c,

the compressive strength of the composites increased markedly with rising ZnO content. The maximum compressive strength reached 25.2 MPa for ZnO content of 6 wt.%. This is approximately 150% higher than the unmodified sample, maintaining good fracture strain characteristics. This indicates that the material achieves a good balance between load-bearing capacity and deformation capacity. In the initial elastic stage, a higher ZnO content results in a steeper slope (higher elastic modulus), which is consistent with the observations from SEM, indicating that ZnO fillers occupy the pores and increase the density. The results confirm that ZnO effectively enhances the rigidity of the substrate. After entering the yield stage, the specimens with higher ZnO content exhibit a flatter yield plateau curve, indicating that ZnO particles hinder microcrack propagation by inhibiting stress transfer at the interface, thereby delaying plastic deformation. Combined XRD and UV-Vis characterization verified that ZnO was well crystallized and uniformly dispersed within the composite. Robust interfaces formed between ZnO, epoxy resin, and straw fibers (Figure 3), providing a structural basis for efficient stress transfer. In the densification regime, specimens with higher ZnO content displayed a prolonged strain-hardening behavior. This demonstrates that the ZnO reinforcement network suppresses initial defects via physical filling, and dissipates mechanical energy under compression through particle rearrangement and interfacial interactions. Upon exceeding ultimate strength, high-ZnO specimens exhibited a gradual stress drop without brittle fracture, revealing excellent damage tolerance. ZnO boosts compressive strength and structural stability through pore filling, interfacial bonding, and effective stress transfer, while retaining deformability. These results validate the potential of straw/epoxy composites for structural load-bearing applications. Future work will evaluate flexural and tensile properties to assess their practical reliability.

To investigate the effect of ZnO content on the surface hydrophobicity of composite materials, contact angle measurements were conducted on straw-based composites with varying ZnO additions (0, 2, 4, 6 wt.%). As shown in Figure 5, the static water contact angle increased from 67.24° to 93.51° with increasing ZnO content, indicating that the surface properties are gradually transitioning from hydrophilic to hydrophobic. This transformation is attributed to the incorporation of ZnO particles, forming micro-nanoscale roughness on the surface of the composite material (consistent with the observed evolution of surface morphology via SEM). According to the Wenzel–Kasi model, the resulting surface roughness intensifies the influence of surface chemistry on wetting behavior. Furthermore, MDI-mediated chemical modification of the ZnO surface proves to be a decisive factor. Forming a dense, low-surface-energy molecular layer on the surface of ZnO particles by chemical bonding or physical adsorption, the substance converts the originally polar ZnO surface into a nonpolar, hydrophobic interface. Increasing ZnO content resulted in more surface-modified ZnO particles being concentrated and distributed in the surface layer of the composite, thereby allowing the low surface energy effect to dominate at a broader scale and significantly reducing the overall surface energy of the composite. The synergistic effect is most pronounced with surface micro-nanoscale roughness and a low-surface-energy chemical state at 6 wt.% ZnO, resulting in optimal hydrophobic properties. Results indicate that regulating the amount of ZnO loading and incorporating surface modification effectively tunes the wettability of the composite material, providing a feasible pathway for engineering functional properties ranging from hydrophilic to hydrophobic.

Figure 6 shows the relationship between ZnO content (0–6 wt.%) and the water absorption weight gain of straw-based composites (soaked for 48 h). As the ZnO content increases, the water absorption weight gain of the composites gradually decreases from approximately 1.63% to 1.13%. This indicates that the incorporation of ZnO significantly improves water resistance. As shown in Figure 3, ZnO particles effectively occupy interfacial voids and microdefects within the straw fiber matrix, forming a denser internal structure,

thereby physically blocking the microscopic pathways enabling water penetration. Additionally, XRD and UV-Vis spectroscopic investigations confirm that ZnO achieves excellent crystallinity and uniform dispersion in this composite system (Figure 3). The interfacial bonding between ZnO and the matrix is strengthened by physical adsorption and potential coordination interactions, thereby reducing capillary water absorption pathways caused by weak interfacial bonding. Crucially, contact angle measurements (Figure 5) indicate that the composite surface transitions from hydrophilic (67.24°) to hydrophobic (93.51°) as the ZnO content increases. This variation arises from the synergistic effect of the low-surface-energy molecular layer formed by the surface chemical modification of ZnO and the micro- and nano-scale surface roughness. Consequently, the hydrophobic surface reduces the tendency of water to wet and adhere to the material surface, thereby hindering moisture penetration from the surface into the interior. In conclusion, the incorporation of ZnO systematically enhances the water resistance of straw-based composites via three mechanisms: pore filling, interfacial reinforcement, and surface hydrophobicity. This series of interactions establishes a critical materials foundation for their applications in humid environments.

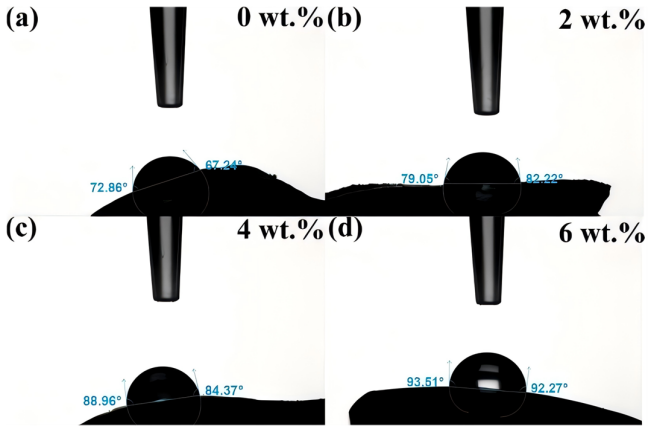


Figure 5. Static Water Contact Angles of the Composites with Different ZnO Additions: (**a**) 0 wt.%; (**b**) 2 wt.%; (**c**) 4 wt.%; and (**d**) 6 wt.%, respectively.

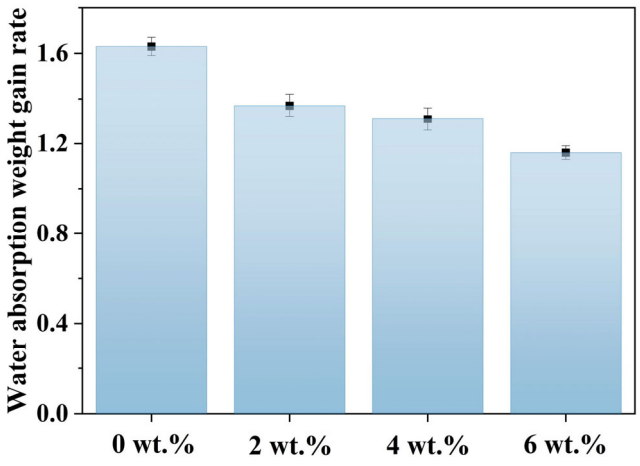


Figure 6. Effect of ZnO Addition on the Water Absorption and Weight Gain Rate of Straw-Based Composites.

3.3. Mechanism Behind the Enhanced Performance of Straw-Based Composites

Differential scanning calorimetry (DSC) revealed the complex effects of varying ZnO content on the state of water and the crystallization behavior of wax in straw-based composites, as shown in Figure 7. DSC characterization revealed a distinct endothermic peak centered at 61 °C, which was attributed to the melting of natural wax components within

the straw. When 2 wt.% ZnO was incorporated, the melting enthalpy of the wax exhibited a remarkable decline from −11.11 J/g to −8.59 J/g, with a corresponding reduction rate of 23%. This reduction indicates that an appropriate amount of ZnO can suppress the ordered arrangement and crystallization of wax molecules through interfacial interactions. The result is further supported by the enhanced interfacial bonding observed via SEM and the good dispersion of ZnO observed via XRD. However, further increasing the ZnO content to 6 wt.% caused the melting enthalpy and peak temperature to return to levels similar to the unmodified sample. The underlying mechanism still requires further investigation, and factors contributing to this include the dispersion state of ZnO, interfacial interactions, or changes in polymer chain mobility. In addition, the exothermic peak observed at approximately −7 °C corresponds to the crystallization process of the water capable of freezing within the system. The crystallization enthalpy of free water decreased from 2.30 J/g to 1.35 J/g and 1.28 J/g, respectively, as the ZnO content increased to 2 wt.% and 4 wt.%. This indicates that the introduction of ZnO significantly reduces the free water content in the material, which is attributed to the physical occupation of pores and interfaces by ZnO, thereby reducing the available sites for water storage. In contrast, the enthalpy of crystallization of the 6 wt.% sample increased slightly, which is consistent with the restoration of waxy behavior. This phenomenon results from interface inhomogeneity caused by filler agglomeration. The findings indicate that ZnO exhibits non-monotonic behavior influencing wax crystallization and the state of water in the composite material. An optimal addition level (2–4 wt.%) can synergistically inhibit wax crystallization and reduce the free water content, facilitated by interface modification and structural filling. However, excessive addition (6 wt.%) may lead to partial phase separation from filler aggregation, thereby partially offsetting the aforementioned improvements. This finding validates the previously observed behavior in mechanical properties, thermal stability, and hydrophobicity, demonstrating that the dispersion state and interfacial structure of the filler are critical factors controlling the multi-scale properties of straw-based composites.

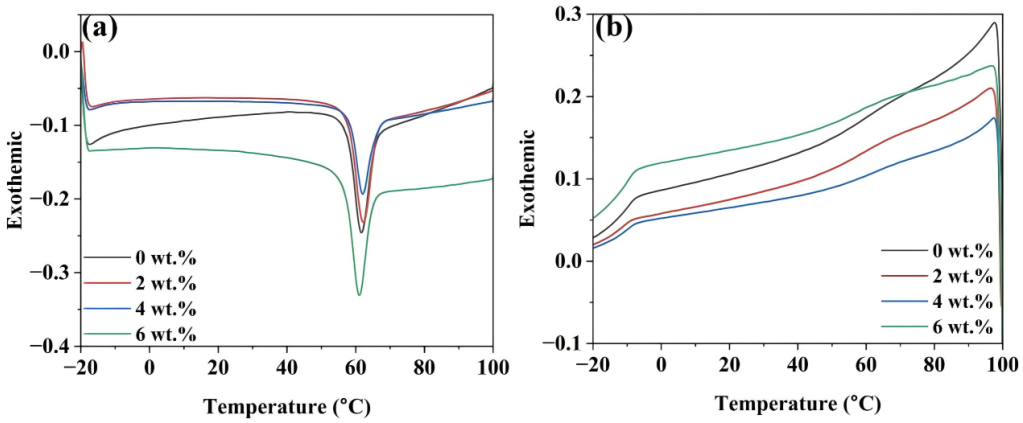


Figure 7. DSC Curves of Straw-Based Composites with Different ZnO Additions: (**a**) Heating scan and (**b**) cooling scan.

The bonding structure of straw-based composites with different ZnO contents was analyzed using X-ray photoelectron spectroscopy (Figure 8). All samples exhibited a broad main peak at approximately 532.6 eV in the O 1 s spectrum. This peak primarily arises from the overlapping signals of oxygen-containing functional groups in the organic matrix, such as C-O-C (MDI) and C-O-H/C-O-C (straw cellulose). The peak is relatively intense, indicating that the organic matrix completely covers the surface of the ZnO filler within the XPS penetration depth (approximately 10 nm). The shift of the C–O peak toward the low-binding-energy region indicates that ZnO modification increases the elec-

tron density on the straw surface, resulting in an electron-rich surface. This observation is consistent with the SEM morphology, the latter also showing ZnO dispersed within the matrix. In the C 1 s spectrum, the following two peaks were observed: C-C/C-H (284.8 eV) and C-O (286.3 eV). As the ZnO content increased, the relative intensity of the C-O peak exhibited a non-monotonic trend, with an initial increase followed by a decrease. The results indicate that ZnO interacts with oxygen-containing groups at the interface via coordination and hydrogen bonding, thereby influencing the chemical environment of the organic layer on the surface and facilitating its cross-linking. Notably, the Zn $2p_{3/2}$ characteristic peak at 1022.48 eV was observed in all ZnO-containing samples. This peak exhibits a positive shift of approximately 0.7 eV compared to the standard value for pure ZnO (approximately 1021.78 eV), accompanied by a broadening of the peak width. This chemical shift conclusively demonstrates the presence of electronic interactions between ZnO and the organic matrix. The enhanced activity may be attributed to interfacial interactions between Zn and oxygen-containing functional groups in the straw components (Zn-O-C) or to surface hydroxylation (Zn-OH) [36,37]. Consequently, the hydroxylation of the ZnO surface leads to a local redistribution of charge. The interfacial chemical bonding mechanism explains the improvements in thermal stability (Figure 4b), mechanical properties (Figure 4c), and hydrophobicity (Figure 5) of ZnO-modified composites at the molecular level. Suitable interface interactions can enhance stress transfer, restrict thermal motion of polymer chains, and synergistically promote hydrophobic surface modification. In contrast, aggregate formation caused by excessive ZnO (e.g., 6 wt%) may affect the uniformity of these interactions, leading to a stepwise decline in performance metrics. XPS analysis confirmed that ZnO was successfully incorporated into the composite materials, a finding evidenced by the surface chemical state, and revealed the presence of significant interfacial electronic coupling between ZnO and the organic phase. Overall, these findings provide strong chemical evidence for the role of ZnO in reinforcing and modifying straw-based composites across multiple scales, highlighting a key contribution to enhancing composite performance and broadening application possibilities.

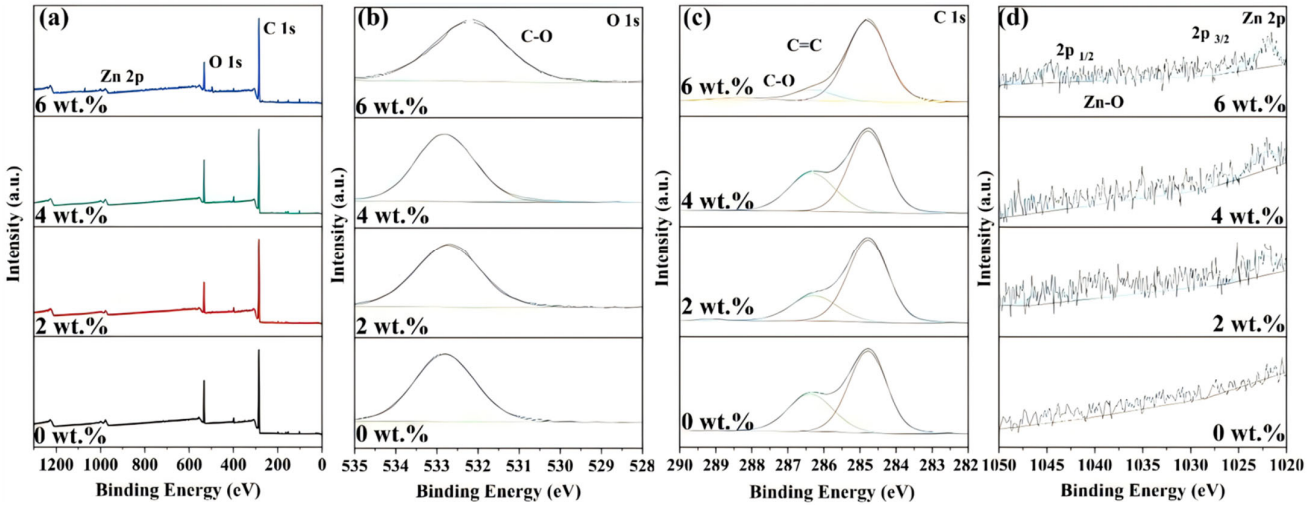


Figure 8. Effect of ZnO Addition on the XPS Spectra of Straw-Based Composites: (**a**) Survey, (**b**) O 1s orbital, (**c**) C 1s orbital, (**d**) Zn 2p orbital.

Figure 9 shows transmission electron microscopy (TEM) images of the straw-ZnO composite. These images directly demonstrate the effect of ZnO incorporation in regulating the microstructure of the straw-based composite. In Figure 9a, the morphology of pure straw powder is shown. It exhibits a smooth surface and lacks a long-range ordered crystal lattice structure, displaying the typical characteristics of amorphous biomass fibers, which

is consistent with the observation of broad, diffuse diffraction peaks in the XRD analysis. In contrast, Figure 9b shows the composite sample containing 6 wt.% ZnO, revealing a large number of nanoparticles adhering to the surface of the straw fibers. These particles exhibit a uniform size distribution, and no significant aggregation is observed. These particles exhibited distinct diffraction fringes, with interplanar distances measured at 0.242 nm and 0.285 nm, corresponding to the (101) and (100) crystal planes of hexagonal magnesium aluminate-type ZnO (PDF# 36-1451). This result directly confirms that highly crystalline ZnO nanoparticles have been successfully loaded onto the surface of straw fibers. The uniform distribution of ZnO nanoparticles enables them to form strong interfacial bonds with straw fibers, thereby creating physical cross-linking points. These cross-linking points serve to refine the microstructure of the composite material and inhibit the propagation of microcracks. Simultaneously, the high modulus of ZnO grains effectively transmits and distributes stress exerted on the material, thereby enhancing its overall mechanical strength. The well-defined lattice structure indicates that the ZnO nanoparticles maintain high crystallinity, and the tight contact at the interfaces reveals strong interactions between the ZnO and the straw. This microstructural feature is consistent with the observations reported in the aforementioned study: the compressive strength of the composite increases significantly with increasing ZnO content (Figure 4c), revealing the structural mechanism underlying the enhancement of the mechanical properties of straw-based composites by ZnO at the nanoscale.

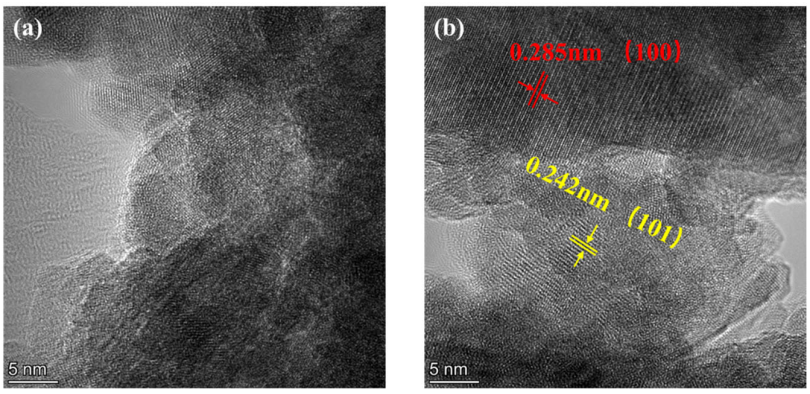


Figure 9. HRTEM Images of Straw-Based Composites with Different ZnO Additions: (**a**) 0 wt.%; (**b**) 6 wt.%.

Figure 10 shows the electron paramagnetic resonance (EPR) spectra of straw-based composites with varied ZnO concentrations (0–6 wt.%). The spectra reveal the influence of ZnO incorporation on the behavior of active radicals (·OH) in the materials. The EPR signal intensity of the pure straw matrix (0 wt.% ZnO) is notably low, exhibiting an almost horizontal baseline. The results indicate that, under ZnO-free conditions, the concentration of detectable paramagnetic centers is very low at the initial stage. As the ZnO content gradually increases to 6 wt.%, a well-defined EPR signal peak appears near $g \approx 2.003$, exhibiting a continuous increase in intensity. The signal is attributed to carbon-centered or oxygen-vacancy-related free radicals formed within the material. It exhibits a monotonic increase in intensity with elevated ZnO content, demonstrating a significant increase in the concentration of active free radicals [38]. The phenomenon is mainly attributed to the introduction of semiconductor properties in ZnO and interactions at the interface between ZnO and the organic matrix. As a wide-bandgap semiconductor, the surface of ZnO and the ordered lattice can act as ferromagnetic centers. Moreover, the presence of ZnO facilitates the cleavage of chemical bonds (C–O, C–C) in the organic components of straw and accelerates redox reactions. This process arises from the interface charge transfer mechanism,

resulting in the generation of free radicals. The formation of these reactive oxygen species signifies that the composite exhibits electron transfer and redox activity, endowing it with the potential to catalyze radical-mediated oxidation reactions and possibly enhancing anti-oxidative properties. The intensity of EPR signals is correlated positively with the ZnO content, further confirming that ZnO acts as both a structural filler and an electronically active component in this system. From the perspective of free-radical chemistry, this result provides new mechanisms for understanding the functionalization of ZnO-modified rice straw-based composites, consistent with the aforementioned observations regarding UV absorption (Figure 4a) and interfacial enhancement (XPS analysis). The intensified ·OH characteristic signal in the EPR spectrum directly confirms that the electron-rich surface possesses stronger oxygen-activating capabilities.

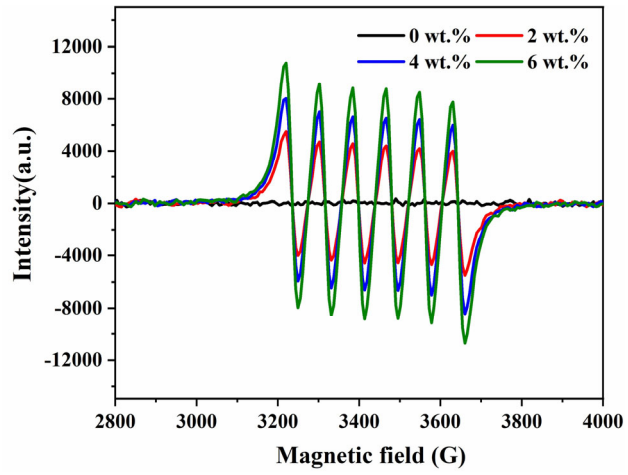


Figure 10. Effect of ZnO Addition on EPR Spectra of Straw−Derived Composite Materials.

3.4. Economic Accounting

We conducted a preliminary economic assessment of raw material costs to serve as a reference indicator for economic feasibility. We consulted relevant market prices and drew on economic analysis methods similar to those used for biomass composites. The raw material cost for this material is approximately 3639 RMB/t (Table 2). Considering additional costs including labor and energy consumption following large-scale production, the final production cost is expected to be around 3800–4200 RMB/t. Currently, traditional outdoor panels on the market are priced at approximately 5000–8000 RMB/t. This suggests that further reducing MDI consumption by optimizing processes (refining hot-pressing parameters and exploring low-cost bio-based adhesives) could make this material competitively priced in the market.

Table 2. Cost Accounting Sheet.

Cost Item	Quantity (kg/t Plate)	Unit Price (RMB/kg)	Cost (RMB/t)
Straw powder	800	0.5	400
MDI	150	18	2700
NaOH	60	0.66	39
Paraffin emulsion	20	8	160
Sulfuric acid	53	0.76	40
Water and Electricity	-	-	300
Total cost	-	-	3639

4. Conclusions

The incorporation of ZnO into straw to modify its characteristics has successfully produced a straw-based composite material with excellent overall performance. The main

conclusions are as follows: Analysis by means of XRD and SEM confirmed that alkali treatment effectively removed a portion of the hemicellulose and lignin from the straw fibers, thereby improving their interfacial compatibility with the epoxy resin matrix. Subsequently, TG analysis revealed that the residual rate after ZnO incorporation was 63.78%. Furthermore, the stress–strain curve displayed a maximum compressive strength of 25.2 MPa at a ZnO content of 6 wt.%, confirming that this material achieves the mechanical performance requirements for commercial furniture applications both indoors and outdoors. This composite material exhibits outstanding multifunctional features. UV-Vis spectroscopic analysis indicates that the addition of ZnO reduces the absorbance of the straw-based composite material in the visible light range of 400–800 nm. Contact angle measurements show that the surface exhibits a contact angle of 93.51° with water, indicating that the material possesses significant hydrophobicity and water repellency. Based on TEM and EPR spectroscopy analyses, these properties are primarily attributed to the synergistic interaction between the effective dispersion of ZnO and the highly cross-linked cellulose network of the straw, along with the generation of active radicals. This study achieved significant improvements in the mechanical strength, water resistance, and UV stability of straw-based composites by optimizing material design and processing techniques, thereby overcoming key performance limitations of traditional outdoor wood, including susceptibility to decay, poor weather resistance, and low straw utilization rates. This approach opens new avenues for the high-value utilization of crop straw and provides innovative research pathways for developing sustainable, durable, and environmentally friendly outdoor furniture, highlighting significant environmental advantages and broad application prospects.

Author Contributions: Conceptualization S.J.; Methodology, Y.L. and Y.F.; Resources, Y.L.; Data curation, S.J. and Y.F.; Writing—original draft, S.J.; Writing—Review and editing, Y.L.; Supervision, Y.L. and Y.F.; Visualization, Y.L. and Y.F.; Project administration, Y.L. All authors have read and agreed to the published version of the manuscript.

Funding: This research received no external funding.

Institutional Review Board Statement: Not applicable.

Informed Consent Statement: Not applicable.

Data Availability Statement: The original contributions presented in this study are included in the article. Further inquiries can be directed to the corresponding author.

Conflicts of Interest: The authors declare that they have no known competing financial interests or personal relationships that could have appeared to influence the work reported in this paper.

References

1. Hamadyk, E.; Amado, M.; Brito, J.D. Use of timber for the sustainable city growth and its role in the climate change. In *Proceedings of the IOP Conference Series: Earth and Environmental Science*; IOP Publishing: Bristol, UK, 2020; Volume 410, p. 012034.
2. Pinno, B.D.; Thomas, B.R.; Lieffers, V.J. Wood supply challenges in Alberta—Growing more timber is the only sustainable solution. *For. Chron.* **2021**, *97*, 106–108. [CrossRef]
3. Hasan, K.M.F.; Horváth, P.G.; Kóczán, Z.; Le, D.H.A.; Bak, M.; Bejó, L.; Alpár, T. Novel insulation panels development from multilayered coir short and long fiber reinforced phenol formaldehyde polymeric biocomposites. *J. Polym. Res.* **2021**, *28*, 467. [CrossRef]
4. Poudel, R.; Karak, N. Sustainable green composite of yam and agricultural waste corn stalk fiber with good mechanical, thermal, optical, aging performance and excellent biodegradability. *Compos. Sci. Technol.* **2023**, *244*, 110276. [CrossRef]
5. John, M.J.; Thomas, S. Biofibres and biocomposites. *Carbohydr. Polym.* **2008**, *71*, 343–364. [CrossRef]
6. Houankpo, T.O.N.; Ma, Z.; Zhao, Z.; Tian, G. Performance of cementitious high-pressure mixtures with wheat and corn straw fiber and straw ashes. *Case Stud. Constr. Mater.* **2025**, *22*, e04175. [CrossRef]

7. Wang, P.; Liu, C.Q.; Chang, J.; Yin, Q.; Huang, W.; Liu, Y.; Dang, X.; Gao, T.; Lu, F. Effect of physicochemical pretreatments plus enzymatic hydrolysis on the composition and morphologic structure of corn straw. *Renew. Energy* **2019**, *138*, 502–508. [CrossRef]
8. Petrella, A.; De Gisi, S.; Di Clemente, M.E.; Todaro, F.; Ayr, U.; Liuzzi, S.; Dobiszewska, M.; Notarnicola, M. Experimental Investigation on Environmentally Sustainable Cement Composites Based on Wheat Straw and Perlite. *Materials* **2022**, *15*, 453. [CrossRef] [PubMed]
9. Daud, Z.; Hatta, M.Z.M.; Kassim, A.S.M.; Awang, H.; Aripin, A.M. Exploring of Agro Waste (Pineapple Leaf, Corn Stalk, and Napier Grass) by Chemical Composition and Morphological Study. *BioResources* **2014**, *9*, 872–880. [CrossRef]
10. Mirițoiu, C.M.; Dobrotă, D.; Popa, D. Designing and study of composites reinforced with shredded corn stalks using a variety of matrices based on dammar, epoxy and acrylic resins. *Polym. Test.* **2025**, *142*, 108672. [CrossRef]
11. Jiang, D.; An, P.; Cui, S.; Sun, S.; Zhang, J.; Tuo, T. Effect of modification methods of wheat straw fibers on water absorbency and mechanical properties of wheat straw fiber cement-based composites. *Adv. Mater. Sci. Eng.* **2020**, *2020*, 5031025. [CrossRef]
12. Abdulqader, A.A. Efficient utilization of corn stalk and poplar planer shavings in manufacturing particleboard. *Maderas. Cienc. Tecnol.* **2021**, *23*, 1–10. [CrossRef]
13. Alshahrani, H.; Arun Prakash, V.R. Mechanical, fatigue and DMA behaviour of high content cellulosic corn husk fibre and orange peel biochar epoxy biocomposite: A greener material for cleaner production. *J. Clean. Prod.* **2022**, *374*, 133931. [CrossRef]
14. Mihajlova, J.; Savov, V.; Simeonov, T. Effect of the content of corn stalk fibres and additional heat treatment on properties of eco-friendly fibreboards bonded with lignosulphonate. *Drewno. Pr. Nauk. Doniesienia. Komun.* **2022**, *65*, 209. [CrossRef]
15. Astari, L.; Belleville, B.; Ozarska, B.; Umemura, K.; Crawford, R.; Kusumaningrum, W.B.; Ismayati, M. Performance of self-binding engineered panels made from sweet corn stalks (*Zea mays* L.) for furniture applications. *Bioresour. Technol. Rep.* **2024**, *25*, 101802. [CrossRef]
16. Shakir, M.A.; Ahmad, M.I.; Ramli, N.K.; Yusup, Y.; Alosaimi, A.M.; Alorfi, H.S.; Hussein, M.A.; Rafatullah, M. Review on the influencing factors towards improving properties of composite insulation panel made of natural waste fibers for building application. *J. Ind. Text.* **2023**, *53*, 1–33. [CrossRef]
17. Khan, A.; Mishra, A.; Patidar, R.; Pappu, A. Effect of lignocellulosic corn stalk on mechanical, physical, and thermal properties of injection moulded low density polyethylene composites: An approach towards a circular economy. *Heliyon* **2024**, *10*, e25287. [CrossRef] [PubMed]
18. Bheel, N.; Chohan, I.M.; Alwetaishi, M.; Waheeb, S.A.; Alkhattabi, L. Sustainability assessment and mechanical characteristics of high strength concrete blended with marble dust powder and wheat straw ash as cementitious materials by using RSM modelling. *Sustain. Chem. Pharm.* **2024**, *39*, 101606. [CrossRef]
19. Kaya, G.G.; Yilmaz, E.; Deveci, H. Sustainable nanocomposites of epoxy and silica xerogel synthesized from corn stalk ash: Enhanced thermal and acoustic insulation performance. *Compos. Part B-Eng.* **2018**, *150*, 1–6. [CrossRef]
20. Li, Z.; Jin, Q.; Shi, C.; Hu, D. Synergistic mechanisms and mesoscopic failure characteristics of wheat straw powder-enhanced microbial cemented aeolian sand. *Powder Technol.* **2025**, *457*, 120879. [CrossRef]
21. Rabani, I.; Jang, H.N.; Park, Y.J.; Tahir, M.S.; Lee, Y.B.; Moon, E.Y.; Song, J.W.; Seo, Y.S. Titanium dioxide incorporated in cellulose nanofibers with enhanced UV blocking performance by eliminating ROS generation. *RSC Adv.* **2022**, *12*, 33653–33665. [CrossRef]
22. Anwer, M.B.; Shubrem, A.S.; Abdulhaleem, F.A.; Al-Mashhadani, M.H.; Jawad, S.F.; Alyami, M.S.S.; Alshareef, S.A.; Alhuwaymil, Z. An Overview on the Role of Nanoparticles for the UV Shielding of Bio-Based Poly (Lactic Acid) Coupled with Enhanced Physico-Chemical Properties. *J. Vinyl Adit. Technol.* **2025**, *31*, 1286–1302. [CrossRef]
23. Glažar, D.; Tomšič, B.; Jerman, I.; Chouhan, R.S.; Šuligoj, A.; Zorc, M.; Pintar, A.; Kovač, J.; Krajnc, A.; Ruiz-Zepeda, F.; et al. Surface-engineered ag/TiO_2/graphitic carbon nitride nanocomposites on cotton textiles for multifunctional photocatalytic, UV shielding, and antibacterial performance. *Appl. Surf. Sci.* **2025**, *721*, 165446. [CrossRef]
24. Subramaniyan, S.; Liu, Y.; Raina, D.B.; Li, X.Y.; Zhang, B.Z. Bio-sourced aromatic polyesters as non-toxic, non-leachable UV-blockers for sunscreens. *Mater. Today Chem.* **2025**, *43*, 102463. [CrossRef]
25. Cormack, P.A.G.; Erdemli, O.C.; Sankey, S.W. Polymerizable UV absorbers for the UV stabilization of polyesters. I. Design, synthesis and polymerization of a library of absorbing monomers. *Arkivoc* **2021**, *6*, 148–173. [CrossRef]
26. Silva, M.R.F.; Alves, M.F.R.P.; Cunha, J.P.G.Q.; Costa, J.L.; Silva, C.A.; Fernandes, M.H.V.; Vilarinho, P.M.; Ferreira, P. Nanostructured transparent solutions for UV-shielding: Recent developments and future challenges. *Mater. Today Phys.* **2023**, *35*, 101131. [CrossRef]
27. Hegazy, H.A.; Moon, H.H.; Perumal, S.; Elmasry, M.R.; Park, J.; Kim, Y.C.; Song, C. Multifunctionalimidazole-functionalized polyaspartamide/TiO_2 composites for UV screening, heavy metal removal, and suppressed photocatalytic activity. *Results Chem.* **2025**, *18*, 102765. [CrossRef]
28. Ponte, C.; Grosche, L.C.; Kolen'ko, Y.V.; Sousa, J.P.S. Efficient UV-shielding coatings with carbon quantum dots. *Sustain. Mater. Technol.* **2025**, *43*, e01301. [CrossRef]
29. Alsukaibi, A.K.D.; Khan, M.W.A.; Al-Otaibi, A.; Alshamari, A.K.; Alshammari, E.M.; Mechi, L.; Alimi, F.R.; Khan, S.N. Modified ZnO mediated dye detoxification by a heterogeneous fenton process. *Emerg. Mater. Res.* **2023**, *12*, 145–153. [CrossRef]

30. Karbalaei, H.; Tarmian, A.; Rasouli, D.; Pourmahdian, S. Effects of UV-curing epoxy acrylate and urethane acrylate coatings incorporated with ZnO nanoparticles on weathering resistance of thermally modified timber. *Wood Mater. Sci. Eng.* **2022**, *17*, 868–877. [CrossRef]
31. Xing, D.; Zhang, Y.; Hu, J.; Yao, L. Highly hydrophobic and self-cleaning heat-treated *Larix* spp. Prepared by TiO_2 and ZnO particles onto wood surface. *Coatings* **2020**, *10*, 986. [CrossRef]
32. Paul, D.; Petrič, M.; Humar, M.; Fabjan, E.Š.; Gaff, M.; Tesařová, D. Enhancing the superhydrophobicity, UV-resistance, and antifungal properties of natural wood surfaces via in situ formation of ZnO, TiO_2, and SiO_2 particles. *Nanotechnol. Rev.* **2025**, *14*, 20250171. [CrossRef]
33. Nagarajappa, G.B.; Nair, S.; Srinivas, K.; Rao, A.N.S.; Pandey, K.K. Photostability of acetylated wood coated with nano Zinc oxide. *Maderas. Cienc. Tecnol.* **2020**, *22*, 365–374. [CrossRef]
34. Wu, Y.; Wu, X.; Yang, F.; Ye, J. Preparation and characterization of waterborne UV lacquer product modified by Zinc oxide with flower shape. *Polymers* **2020**, *12*, 668. [CrossRef]
35. Kaur, R.; Bhardwaj, S.K.; Chandna, S.; Kim, K.H.; Bhaumik, J. Lignin-based metal oxide nanocomposites for UV protection applications: A review. *J. Clean. Prod.* **2021**, *317*, 128300. [CrossRef]
36. Zhang, X.; Dong, Z.; Liu, S. Maize straw-templated hierarchical porous ZnO: Ni with enhanced acetone gas sensing properties. *Sens. Actuators B Chem.* **2017**, *243*, 1224–1230. [CrossRef]
37. Cole, C.; Shyr, T.; Ou-Yang, H. Metal oxide sunscreens protect skin by absorption, not by reflection or scattering. *Photodermatol. Photo* **2016**, *32*, 5–10. [CrossRef]
38. Arienzo, M.; Mostoni, S.; Crapanzano, R. Insight into the influence of ZnO defectivity on the catalytic generation of environmentally persistent free radicals in ZnO/SiO_2 systems. *Phys. Chem. C* **2019**, *123*, 21651–21661. [CrossRef]

Disclaimer/Publisher's Note: The statements, opinions and data contained in all publications are solely those of the individual author(s) and contributor(s) and not of MDPI and/or the editor(s). MDPI and/or the editor(s) disclaim responsibility for any injury to people or property resulting from any ideas, methods, instructions or products referred to in the content.